In vitro validation of some flow assumptions for the prediction of the pressure distribution during obstructive sleep apnoea

A. Van Hirtum[1] X. Pelorson[1] P. Y. Lagrée[2]

[1]Institut de la Communication Parlée, INPG-Université Stendhal, Grenoble, France
[2]Laboratoire de Modélisation en Mécanique, Université Paris VI, Paris, France

Abstract—*An adequate description of the pressure distribution exerted by the fluid flow on pharyngeal walls is a first requirement to enhance the understanding, modelling and, consequently, the prediction of airway collapse during obstructive sleep apnoea. From a fluid mechanical point of view, several flow assumptions can be formulated to reduce the governing flow equations. The relevance of some major flow assumptions and the accuracy of the resulting flow description with respect to obstructive sleep apnoea was investigated on a rigid geometrical replica of the pharynx. Special attention was given to the influence of geometrical asymmetry and to the position of the flow separation point. An in vitro experimental and theoretical study of steady pharyngeal fluid flow is presented for different constriction heights and upstream pressures. Pressure and velocity distributions along a rigid in vitro replica of the oro-pharyngeal cavity were compared with different flow predictions based on various assumptions. Fluid flow models were tested for volume flow rates ranging from 5 to 120 l min^{-1} and for minimum apertures between 1.45 and 3.00 mm. Two-dimensional flow models were required and predicted experimental results with an accuracy of 15%. Flow theories classically used in the case of a Starling resistor provided poor agreement.*

Keywords—*Upper airway collapse, Obstructive sleep apnoea syndrome, Pressure distribution, Tongue replica, Geometrical asymmetry, Flow separation postition*

Med. Biol. Eng. Comput., 2005, **43**, 162–171

1 Introduction

OBSTRUCTIVE SLEEP apnoea (OSA) is defined as the intermittent cessation of breathing during sleep and is characterised by recurrent collapse of the pharyngeal airway. OSA has been extensively shown to be an important health care issue, with a reported prevalence of 4% in adult men and 2% in adult women (YOUNG *et al.*, 1993). OSA causes excessive daytime sleepiness and increases the development of cardiovascular diseases and arterial hypertension (PEPPARD *et al.*, 2000). Consequently, OSA has adverse consequences on the patient's daily life and is associated with an increased risk of public traffic accidents (FLEMONS and REIMER, 2002; TERAN-SANTOS *et al.*, 1999).

The OSA syndrome is mainly treated using empirical therapeutic or surgical procedures. Long-term use of therapeutic treatment strategies, such as continuous positive airway pressure or pharyngeal appliances, causes daily discomfort and reduces the quality of life (FLEMONS, 2002).

Correspondence should be addressed to Dr Annemie Van Hirtum; email: annemie@icp.inpg.fr

Paper received 9 February and in final form 19 July 2004

MBEC online number: 20053951

The long-term effectiveness of surgical treatment is estimated to range between 50 and 78%, depending on the surgical procedure applied (FLEMONS, 2002; BRIDGMAN and DUNN, 2002; SHER *et al.*, 1996). Therefore current research aims to improve the diagnosis, follow-up and treatment of OSA syndrome. In particular, the need for further understanding of the OSA syndrome to favour successful development of therapeutic and surgical treatments is stressed (FLEMONS, 2002; HUI *et al.*, 2000; LIPTON and GOZAL, 2003; MCNICHOLAS, 2003; PENZEL *et al.*, 2002; RAMA *et al.*, 2002; AYAPPA and RAPOPORT, 2003; PAYAN *et al.*, 2002).

The present study is an essential step towards a physical model of the ongoing flow phenomena. A physical flow model is a first requirement to model the fluid–structure interactions long-term, aiming to predict the outcome of surgical interventions.

The upper airway is a potentially collapsible structure whose patency is dictated by a combination of passive mechanical properties and active neural mechanisms. In particular, OSA syndrome is known to be due to a partial (hypopnoea) or total (apnoea) collapse of the upper airway during inspiration (AYAPPA and RAPOPORT, 2003). The Starling resistor is a classical experiment used to study biofluid mechanical applications involving collapsible structures, such as flow limitation in the airway branches (GROTBERG and JENSEN, 2004; LAMBERT and WILSON, 1972). Owing to the pharyngeal asymmetry in

both geometry and tissue properties (rigid hard palate against soft tissues), the relevance of such devices for the study of OSA is not obvious. An alternative set-up is presented in this paper.

From a physical point of view, neglecting neural mechanisms, the airway collapse is due to the fluid-mechanical interaction of the fluid (airflow during inspiration) and the surrounding structure (tissues). Studies of the biomechanical pharyngeal airflow and resulting forces in cases of OSA are very limited. Because of a wide clinical interest, most of the literature in the field concentrates on the relationship between inspiratory and expiratory pressure and the volume flow velocity.

Usually, the pressure–flow relationship in the upper airway is mathematically fitted by a quadratic or polynomial function so as objectively to detect inspiratory flow limitation and related phenomena (HENKE, 1998; MANSOUR *et al.*, 2002). The resulting pressure–flow relationship obtained by curve fitting of the applied mathematical polynomial or quadratic formulation may provide useful empirical information, but does not describe the complexity of the ongoing physical flow behaviour and does not inform on the pharyngeal pressure distribution.

The interaction between the fluid and the surrounding upper airway tissue is expressed by the force exerted by the fluid on the surrounding tissue. This force is determined by the pressure distribution. Therefore, not only does the volume flow velocity need to be accurately predicted from the upstream pressure, as was the aim in HENKE (1998) and MANSOUR *et al.* (2002), but also the pressure distribution along the upper airway. With respect to an accurate description of the pressure distribution, it is generally accepted that an accurate prediction of flow separation is crucial (MATSUZAKI and FUNG, 1976; PEDLEY and LUO, 1998).

A three-dimensional computational simulation of airflow characteristics, including both volume flow velocity and pressure distribution, in an anatomically accurate rigid human pharynx geometry is assessed in SHOME *et al.* (1998). The airflow was assumed to be incompressible and steady. The pressure drop in the pharynx was quantified to lie in the range of 200–500 Pa, provoking the pharynx to collapse. The switch from laminar to turbulence flow was found to increase the pressure drop by 40%. Subtle effects on the airway morphology, as introduced by surgical treatment of OSA, were shown to have a great effect on the pressure drop.

The work presented was intended to contribute to the understanding of flow-induced pharyngeal airway obstruction at the origin of OSA. The pressure distribution along a rigid *in vitro* geometrical constriction, representing the pharyngeal cavity, was predicted from the upstream pressure and geometric information. Several assumptions about the flow and the constriction geometry were experimentally assessed. The model performance of corresponding flow models with increasing complexity was systematically and quantitatively validated.

2 Theory

2.1 *Assumptions and dimensional numbers*

From a fluid mechanical point of view, several flow assumptions can be formulated on the basis of a dimensional analysis of the governing flow equations. This yields a set of non-dimensional numbers that can be interpreted as a measure of the importance of various flow effects. Based on the obtained orders of magnitude for the characteristic non-dimensional numbers, approximations are made to describe the flow. Concerning obstructive sleep apnoea, four non-dimensional numbers were derived based on characteristic conditions listed in Table 1. Physiological data were obtained from *in vivo* observations (LEITH, 1995; MAYER *et al.*, 1996; SCHWAB *et al.*, 1990).

Table 1 Characteristic conditions during obstructive sleep apnoea.

L_0	Tongue length	5 cm
W_0	Pharyngeal width	3 cm
h_0	Minimum aperture	2 mm
c_0	Speed of sound	350 m s^{-1}
ρ_0	Mean density	1.2 kg m^{-3}
μ_0	Dynamic viscosity	1.5×10^{-5} m^2 s^{-1}
t_0	Period of breathing (inspiratory)	4 s
U_0	Flow velocity*	8 m s^{-1}

*Estimated from typical volume flow velocity of 30 l min^{-1}

First, the squared value of the Mach number $Ma = U_0/c_0$, the ratio of flow velocity U_0 to the speed of sound c_0, indicates the tendency of the flow to compress as it encounters a solid boundary. As the velocities involved during respiration are small compared with the speed of sound in air ($Ma_0^2 \approx O(10^{-4})$), the flow is assumed to be incompressible. Secondly, the Strouhal number $Sr = L_0/t_0U_0$ is a dimensionless frequency indicating the ratio of the distance over which flow is convected in a characteristic time t_0 to a characteristic width L_0 of a structure exposed to the flow. The airflow can be considered as primarily steady as long as the flow patterns at any given time are approximately the same, which is reasonable during quiet breathing at the characteristic respiratory frequencies and with rigid walls expressed by a low Strouhal number $Sr_0 \approx O(10^{-3})$.

The assumptions of incompressible and steady flow are not discussed in this paper. The assumptions are indeed widely accepted in the literature (GROTBERG and JENSEN, 2004; PEDLEY and LUO, 1998; SHOME *et al.*, 1998). Note that, in the case of snoring, these assumptions would certainly be debatable.

Thirdly, the Reynolds number $Re = \rho_0 U_0 h_0/\mu_0$, with U_0 a typical flow velocity, h_0 a typical dimension (such as the pharyngeal minimum aperture), μ_0 the dynamic viscosity and ρ_0 the density, represents the importance of inertial forces with respect to the viscous forces acting on a given fluid element and the length of the pharyngeal replica. In the first approximation, the flow is assumed to be inviscid considering the involved characteristic Reynolds numbers $Re_0 \approx O(10^3)$. Although it can be neglected for the bulk of the flow, viscosity is important near the walls, motivating the application of the boundary layer theory. Next, the occurence of flow separation is a consequence of the viscosity and has a strong influence on flow control (MATSUZAKI and FUNG, 1976; PEDLEY and LUO, 1998). Therefore the flow separation point is either considered to be fixed by an empirical *ad hoc* assumption or is predicted based on physical principles. The relevance of this assumption and its influence on the position of flow separation are extensively investigated in this paper.

Fourthly, the ratio of characteristic geometrical lengths yields information about the dimensionality of the flow. The aspect ratio h_0/W_0 is considered, with h_0 a typical minimum aperture and W_0 a typical width. Following the characteristic ratio $h_0/W_0 = 0.09$ [$h_0/W_0 \ll 1$], the flow is assumed to be completely characterised by a bidimensional flow description in the (x, y)-plane. This assumption is experimentally tested.

In the following Section, different flow descriptions are presented based on the assumptions with respect to viscosity, dimensionality of the flow description and the influence of the asymmetry on the geometric replica. As a result, the flow predictions resulting from different simplifications of the

bidimensional laminar, incompressible and quasi-steady Navier Stokes (NS) equations can be numerically and experimetally validated.

2.2 *Theoretical flow predictions*

The origin of OSA lies in a strong interaction of the fluid and the surrounding tissue, provoking the pharyngeal airway recurrently to collapse during sleep. A first requirement to describe ongoing phenomena is to know the pressure variations through the pharyngeal geometry. As an exact analytical solution for the flow through such a constriction is not available, different flow models and flow assumptions are assessed to estimate the volume flow velocity ϕ and the pressure distribution $p(x)$ as a function of position (BLEVINS, 1992; SCHLICHTING and GERSTEN, 2000).

Once $p(x)$ is known, the force $F(x)$ acting by the airflow on the surrounding tissue of the pharynx is deduced as $F(x) = \int p dS$.

2.2.1 *Bernoulli with ad hoc viscosity correction*

In a first approximation, the flow is assumed to be fully inviscid. The three assumptions of incompressible, quasi-steady and inviscid flow allow the steady one-dimensional (1D) Bernoulli law to be applied

$$p(x) + \frac{1}{2}\rho U(x)^2 = cte \tag{1}$$

to estimate the pressure distribution $p(x)$ along the pharyngeal walls. The volume flow velocity is defined by $\phi(x) = U(x)A(x) = cte$, with $U(x)$ the local flow velocity and $A(x)$ the area along the pharyngeal replica. To be useful, an empirical *ad hoc* correction is needed to the 1D Bernoulli equation to account for the occurrence of flow separation downstream of h_{min}. The jet formation downstream from the point of flow separation is due to very strong viscous pressure losses and reversed flow occuring near the wall and thus cannot be predicted by the Bernoulli law. For a steady flow, the onset of separation coinciding with the separation point is defined as $\partial U/\partial n|_{n=0} = 0$. In the literature, the area associated with flow separation A_s is empirically chosen as 1.2 times the minimum area A_{min} along the replica, i.e. $A_s = cA_{min}$, with $c = A_s/A_{min} = 1.2$ (PAYAN *et al.*, 2002; HOFMANS *et al.*, 2003). The *ad hoc* correction for the 1D Bernoulli equation (1) results in a steady 1D expression for $p(x)$ given in (2), with p_0 and A_0, respectively, the pressure and area upstream of the replica indicated in Fig. 2. The volume flow velocity is estimated is (3). In (2), pressure recovery downstream from the point of flow separation is neglected.

$$p(x) = p_0 + \frac{1}{2}\rho\phi^2\left(\frac{1}{A_0^2} - \frac{1}{A(x)^2}\right) \tag{2}$$

$$\phi = A_s\sqrt{\frac{2(p_0)}{\rho}} \quad A_s = cA_{min} \tag{3}$$

The preceding assumption of inviscid flow is not valid for low Reynolds numbers. This is the case for low flow velocities U and/or small h_{min} values. In this case, an extra Poiseuille term is often added to the Bernoulli expression for $p(x)$ in (2) to correct for viscous pressure losses. The Bernoulli expression with Poiseuille correction is given in (4), with μ the dynamic viscosity coefficient, D the diameter of the half cylinder, and $h(x)$ the height between the half cylinder and the flat plate, as defined in Section 3.1.

$$p(x) = p_0 + \frac{1}{2}\rho\phi^2\left(\frac{1}{A_0^2} - \frac{1}{A(x)^2}\right) - \frac{12\mu\phi}{D}\int\frac{dx}{h(x)^3} \tag{4}$$

2.2.2 *Boundary layer solution*

In the preceding Section 2.2.1, the viscosity is either neglected (Bernoulli in (2)) or corrected with an additional Poiseuille term, assuming a fully developed Poiseuille flow (Poiseuille in (4)). However, at high Reynolds numbers, the region in which viscous forces are important is confined to a thin layer adjacent to the wall, which is referred to as laminar boundary layer δ. Outside the boundary layer, the inviscid irrotational main flow, with velocity $U(x)$, is described by Bernoulli equation (3). The resulting boundary layer theory is described by the Von Kármán momentum integral equation for steady flows (SCHLICHTING and GERSTEN, 2000). An approximated method to solve this equation for laminar, incompressible, bidimensional (x, y) boundary layers is given by the Thwaites method.

We introduce two shape parameters $H(\lambda) = \delta_1/\delta_2$, $S(\lambda) \propto \tau_S\delta_2/U$, which are only functions of the velocity profile determined by the acceleration parameter $\lambda \propto (dU/dx)\delta_2$, with $\tau_S(x) \propto \lim_{n\to 0}\partial u/\partial n$ the wall shear stress indicating the viscous force per unit area acting at the wall, the displacement thickness δ_1

$$\delta_1(x) = \int_0^\infty\left(1 - \frac{u(y)}{U}\right)dy \tag{5}$$

and the momentum thickness δ_2

$$\delta_2(x) = \int_0^\infty\frac{u(y)}{U}\left(1 - \frac{u(y)}{U}\right)dy \tag{6}$$

The Von Kármán equation is then approximated by

$$\delta_2^2(x)U^6(x) - \delta_2^2(0)U^6(0) \propto \int_0^x U^5(x)\,dx \tag{7}$$

Equation (7), in combination with the fitted formulas for $H(\lambda)$ and $S(\lambda)$ tabulated in BLEVINS (1992), enables us to compute the desired pressure distribution $p(x)$ up to the flow separation point, where $\tau_S = 0$ for a given input pressure and known geometry. Moreover, the point of flow separation x_S is numerically estimated, as separation is predicted to occur at $\lambda(x_S) = -0.0992$ (PELORSON *et al.*, 1994). Therefore no *ad hoc* assumption is made to account for flow separation.

In DEVERGE *et al.* (2003), the method was successfully applied to predict accurately the position of flow separation and associated pressure within the glottis. In the present study, the prediction of the pressure distribution along the pharyngeal replica is assessed. As flow prediction downstream from the position of flow separation is not possible in the following Sections, two numerical methods of flow prediction are outlined.

2.2.3 *Reduced Navier Stokes*

A second simplification of the Newtonian steady laminar incompressible bidimensional Navier Stokes (NS) equations is obtained by making two additional assumptions. First, the flow is assumed to be characterised by a large Reynolds number, and, secondly, the geometrical transverse dimension (y-axis) is assumed to be small compared the

longitudinal dimension (x-axis). In the geometry under study, the last assumption coincides with $h_0 \ll D$. Applying those assumptions to the bidimensional NS equations results in a system in which the transverse pressure variations are neglected. This system is referred to as the reduced Navier Stokes/Prandtl (RNSP) system, in accordance with Prandtl's formulation of the steady boundary-layer. Non-dimensional variables are obtained by scaling u^* with U_0, v^* with U_0/Re, x^* with $h_0\,Re$, y^* with h_0 and p^* with ρU_0^2 with the Reynolds number defined as $Re = U_0 h_0/\nu$. In terms of the non-dimensional variables, the resulting RNSP equations become

$$\frac{\partial}{\partial x}u + \frac{\partial}{\partial y}v = 0 \quad u\frac{\partial}{\partial x}u + v\frac{\partial}{\partial y}u = -\frac{\partial}{\partial x}p + \frac{\partial^2}{\partial y^2}u \qquad 0 = -\frac{\partial}{\partial y}p \tag{8}$$

The no-slip boundary condition is applied to the lower and upper walls. As the lower wall of the geometry of interest corresponds to $y = 0$, and the distance to the upper wall is denoted by $h(x)$, the no-slip condition becomes, respectively, $(u(x, y = 0) = 0,\ v(x, y = 0) = 0)$ and $(u(x, y = h(x)) = 0,\ v(x, y = h(x)) = 0)$. To solve the RNSP equations numerically, the pressure at the entrance is set to zero, and the first velocity profile needs to be known (Poiseuille). There is no output condition.

3 Materials

To enable experimental validation of the predicted pressure distribution for a given pressure, a suitable *in vitro* pharyngeal replica and experimental set-up are required.

3.1 *In vitro pharyngeal tongue replica*

The place of obstruction in the pharynx at the origin of OSA is known to be very variable (naso-, oro- or laryngopharynx) (RAMA *et al.*, 2002). Regardless of the precise location of the obstruction in the pharynx, the relevant anatomy is imitated *in vitro* by a rigid half cylinder, representing roughly the tongue geometry, placed inside a rectangular uniform pipe representing the pharyngeal wall.

Changing the minimum aperture (h_{min}) between the tongue replica and the pipe allows the study of different anatomical conditions. Consequently, the important geometrical parameters are the diameter D of the half cylinder and the value of h_{min}. In this study, the diameter D of the rigid replica was fixed to 49 mm, which is in accordance with anatomical *in vivo* values. Different degrees of constriction were studied by changing h_{min} between the half cylinder and the flat plate. Minimum distances h_{min} of 1.45, 1.90, 2.30 and 3.00 mm were considered. These distances were measured using calibrated plates with an accuracy of 0.01 mm. To connect the replica to the experimental set-up described in Section 3.2, a triangular attachment of length 25 mm and height 6 mm was fastened to the upper part of the half cylinder, maintaining a fixed vertical height of $h_0 = 34$ mm between the beginning of the attachment and the flat plate. A photograph and longitudinal cross-section of the resulting pharyngeal geometry comprising the attachment and *in vitro* tongue replica are depicted in, respectively, Figs 1 and 2 for the assessed h_{min}'s. The flat plate coincides with the x-axis at $y = 0$. The changing height of the replica along the x-axis is further denoted by $h(x)$. Note the physiologically observed strong asymmetrical nature of the replica's geometry in the (x, y)-plane. The replica has a fixed width W of 34 mm along the z-dimension.

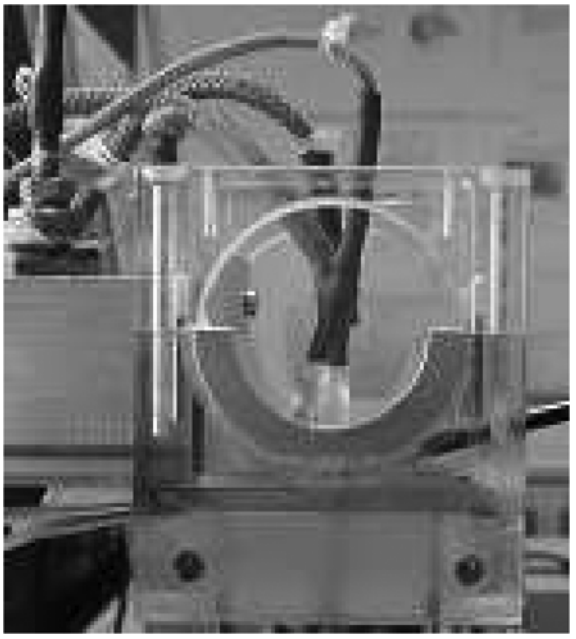

Fig. 1 *Photograph of in vitro pharyngeal tongue replica, mounted pressure transducers and hot film*

3.2 *Experimental set-up*

To simulate the origin of OSA, the rigid pharyngeal replica was attached to an *in vitro* test-installation. The test-installation enabled us to study the influence of various incoming (inspiration) pharyngeal airflow conditions. To validate theoretical flow predictions, flow characteristics were measured at different positions along and upstream from the tongue replica. Incoming airflow conditions were determined by measuring the volume flow velocity ϕ and upstream pressure p_0, as indicated in Fig. 2. The volume flow velocity ϕ ($l\,min^{-1}$) was measured using a thermal mass flow meter* with an accuracy of $0.01\,min^{-1}$. Flow pressure measurements (Pa) were performed at three different positions (p_1, p_2, p_3), depicted in Fig. 2, along the converging part of the rigid tongue replica and the flat bottom plate. The pressure was measured with piezoresistive pressure transducers† positioned in pressure taps of 0.4 mm diameter at the mentioned sites, which allowed dynamic pressure measurements. The site p_3 corresponded to the position h_{min}. The sites p_2 and p_1 were respectively, located upstream from the site p_3 at 4.5 mm and 8.0 mm along the x-dimension. The pressure transducers were calibrated against a water manometer with an accuracy of 1 Pa. The volume flow velocity ϕ and pressure distribution $p(x)$ along the replica were predicted from the measured upstream pressure p_0.

Next to pressure measurements, a constant temperature anemometer system‡ is available in the test-installation to perform flow velocity measurements with an accuracy of $0.1\,m\,s^{-1}$. Velocity profiles can be obtained by moving the hot film using a two-dimensional stage positioning system**. The accuracy of positioning in the x- and y-direction was, respectively, 4 and 2 μm.

*TSI 4040
†Endevco 8507C or Kulite XCS-093
‡IFA 300
**Chuo precision industrial co. CAT-C, ALS-250-C2P and ALS-115-E1P

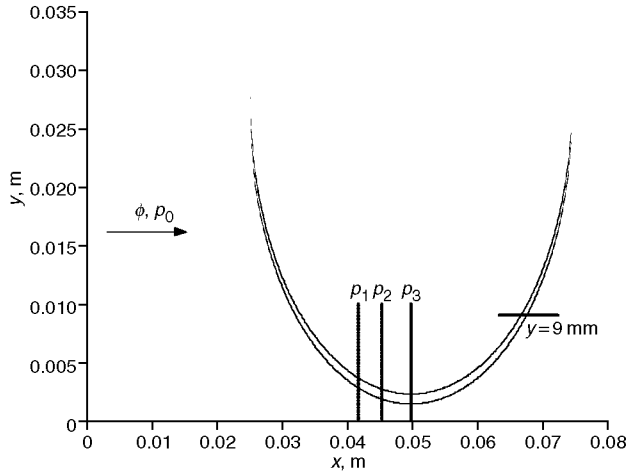

Fig. 2 *Schematic overview of in vitro pharyngeal tongue replica, mounted pressure transducers and hot film. Pharyngeal cavity geometry is represented by flat bottom plate corresponding to $y = 0$ and half cylinders with diameter $d = 49$ mm for assessed h_{min}'s (1.45, 1.90, 2.30 and 3.00 mm). y-axis corresponds to distance between flat plate and half cylinder. x-axis represents distance along longitudinal axis of replica. Sensor sites are indicated with solid line. Direction of incoming airflow is indicated by arrow.*

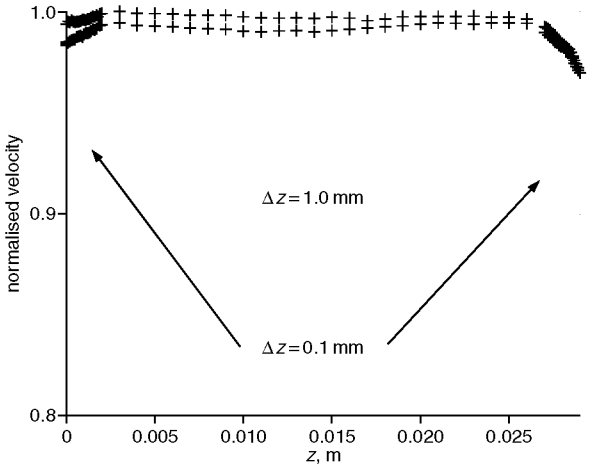

Fig. 3 *Normalised horizontal velocity profile (0 up to 30 mm and 30 down to 0 mm) for $h_{min} = 2.3$ mm and steady flow of 60 l min^{-1}*

4 Predictive performance

The performance of the distinct flow predictions defined in Section 2.2 is statistically quantified by the coefficient of determination R^2 $(0 \leqslant R^2 \leqslant 1)$

$$R^2 = 1 - \frac{\hat{\sigma}^2}{\sigma_y^2} \tag{9}$$

where $\hat{\sigma}^2$ is the sample variance of the prediction residuals, and σ_y^2 is the sample variance of the measured output about its mean value. Larger R^2 values correspond to increased predictive model performance.

5 Results and discussion

The flow predictions outlined in Section 2.2 were developed assuming particular flow conditions. Therefore the major flow assumptions discussed and justified in Section 2.1 were experimentally validated before the predictive value of the flow descriptions was systematically explored, as described in the following Sections.

5.1 *Experimental validation of some major flow assumptions*

5.1.1 *Spatial distribution of the flow*

The steady flow models presented in Section 2.2 resulted in a 1D, quasi-2D or 2D flow description. The third dimension (z-axis), perpendicular to the (x, y)-plane, was assumed to have no influence on the flow. To validate this assumption, the horizontal velocity profile was measured for each h_{min}. Fig. 3 illustrates an sample velocity profile for $h_{min} = 2.3$ mm and a steady flow of 60 l min^{-1}. The step Δz at the edges near the wall is 0.1 mm; elsewhere, Δz equals 1.0 mm.

The anemometer was positioned as close as possible to the minimum aperture. The measured velocity had a standard deviation ($\xi(\%)$) $\xi < 1\%$ around its mean value. $\xi < 1\%$ corresponded to a flat velocity profile along the z-direction. For all assessed apertures and volume flow rates, $\xi < 1\%$ was maintained. At the edges, where a smaller stepsize of $\Delta z = 0.1$ mm was applied, the measured velocities were slightly decreased, owing to the presence of the boundary layer. Consequently, neglecting the z-dimension in the flow description was positively validated, and, as such, a bidimensional (x, y) spacial distribution of the flow was justified motivated.

The velocity profiles depicted following the y-dimension in Fig. 4 draw attention to the asymmetry of the flow within the pharyngeal replica. The vertical velocity along the y-dimension was measured, and the x-value coincides with an aperture of 9 mm along the diverging side of the replica. This position is indicated by the horizontal line at $h(x) = y = 9$ mm in Fig. 2. The vertical velocity profile is measured with a spatial resolution of $\Delta z = 0.1$ mm. Fig. 4 shows the vertical velocity profile for volume flow velocities ranging from 20 l min^{-1} up to 100 l min^{-1} for a minimum aperture $h_{min} = 2.30$ mm; $y = 0$ corresponds to the flat plate of the replica. For high-volume flow velocities, the vertical velocity profiles in Fig. 4 become asymmetrical.

To evaluate the impact of the asymmetry on the pressure distribution, the pressure was measured at positions p_1, p_2 and p_3 on the half cylinder, as well as on the flat bottom plate, as indicated in Fig. 2. Fig. 5 represents an example of the normalised pressure measurements for different values of the upstream pressure p_0 for the minimum aperture, $h_{min} = 3.00$ mm. At the position of the minimum aperture, the ratio p_3/p_0 approximates to -0.15 for both the pressures measured on the half

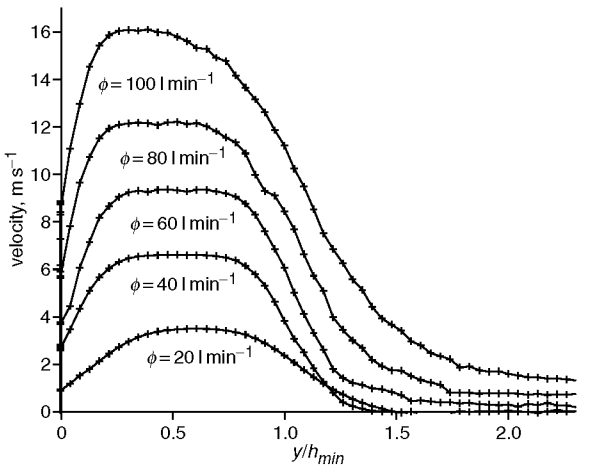

Fig. 4 *Measured vertical (y-axis) velocity profile at $y = 9$ mm for given flow velocities ϕ with $h_{min} = 2.30$ mm. Note asymmetrical behaviour for $\phi = 100$ l min^{-1}*

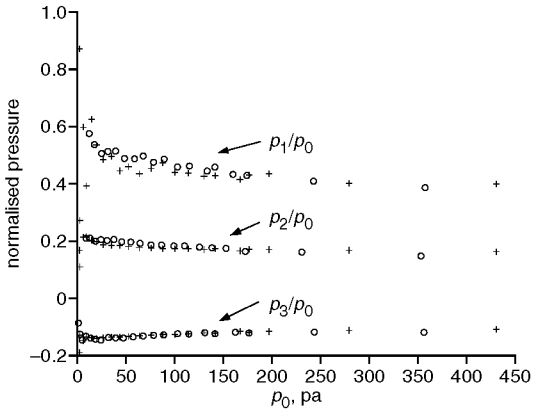

Fig. 5 *Pressure measurements at p_1, p_2 and p_3 normalised with upstream pressure p_0 for $h_{min} = 3.00$ mm. Pressures are measured on (+) half cylinder and on (○) flat bottom plate*

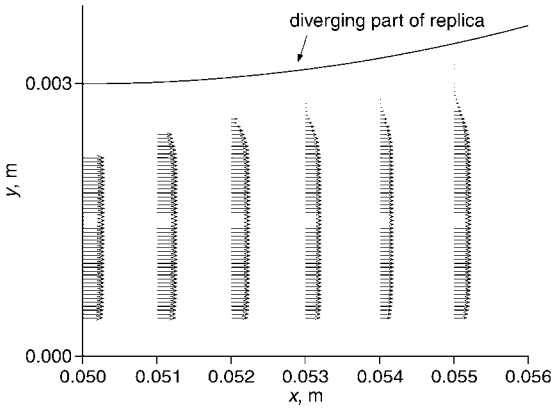

Fig. 6 *Measured bidimensional velocity profile (absolute value) illustrating flow separation and jet formation along diverging part of replica for steady flow of 40 l min^{-1} and $h_{min} = 3.00$ mm. Step of $\Delta x = 1$ mm in x-direction and $\Delta y = 0.05$ mm in y-direction is applied*

cylinder and on the flat bottom plate. This ratio is of the same order of magnitude as the one mentioned in HOFMANS *et al.* (2003) for a symmetrical lip replica with a comparable minimum aperture of $h_{min} = 3.36$ mm. Thus, at the position of minimum aperture, the measured pressure difference between the half cylinder and the flat plate is very limited.

The pressures measured at the flat plate at position p_2 are superior by a few percent to the pressures measured at the half cylinder. Looking at the measurements at position p_1, the same finding holds. Furthermore, the transverse pressure difference is found to decrease approaching the minimum aperture. Therefore the influence of the asymmetry on the pressure measurements grows with increasing absolute values of the spatial derivative, although, systematically, the measured pressure gradients at positions p_2 and p_1 are far inferior to 10%, which is small compared with the general accepted error range of 25% (HOFMANS *et al.*, 2003). The same findings hold for all assessed minimum apertures. Therefore it is concluded that, although measurable, the asymmetry hardly affects either the transverse pressure measurements or, consequently, the sought pressure distribution $p(x)$. This finding is important when we consider application of boundary layer theory, because, as expressed in (8), the equations of motion within the boundary layer assume that transverse pressure variations can be neglected.

5.1.2 *Flow prediction*

Fig. 6 illustrates a detailed bidimensional velocity map for a steady flow of 40 l min^{-1} with a minimum aperture of $h_{min} = 3.00$ mm. The presented findings hold for all assessed minimum apertures and volume flow velocities. The anemometer was displaced with a step of $\Delta x = 1$ mm in the x-direction and $\Delta y = 0.05$ mm in the y-direction.

In the same way as for the horizontal velocity profile depicted in Fig. 3, the decrease in velocity towards the edges provides experimental evidence for the existence of the boundary layer. Along the diverging part of the replica, the velocity tended to zero, which experimentally illustrates the impact of flow separation on the flow also mentioned in SHOME *et al.* (1998).

The importance of the boundary layer and flow separation on the bidimensional flow description is further illustrated in Fig. 4. The plotted profiles show the existence of a boundary layer near the edge ($y/h_{min} = 0$) and the formation of a jet, as the velocity tends to 0 as the ratio y/h_{min} becomes superior to 1. The development of the inviscid main flow with increasing volume flow velocity is clearly illustrated. Owing to the importance of the position of flow separation on the flow control in the following, the relevance of the assumption with respect to a fixed or predicted flow separation point is extensively considered with respect to the sought pressure distribution.

The *ad hoc* corrected Bernoulli law with the assumption of a fixed flow separation point described in Section 2.2.1 results in the most simplified prediction of the sought pressure distribution. The application of the one-dimensional pressure prediction is illustrated in Fig. 7 for a minimum aperture $h_{min} = 1.45$ mm. The volume flow velocity ϕ is varied from 5 up to 120 l min^{-1} in steps of 5 l min^{-1} ($Re \leq 4719$). The ratios of the measured and upstream pressures p_0 at the positions p_1, p_2 and p_3 are indicated with crosses. The one-dimensional pressure distribution $p(x)$ is shown for two different positions of flow seperation expressed by two values of the constant $c = A_s/A_{min}$. The constant c is chosen to be 1.2 and 1.05, corresponding, respectively, to the value proposed in literature and the value retrieved from the measured data $c = \sqrt{1 - p_3/p_0} = 1.05$. Note that, in the last case, the modelling performance is optimised by the use of not only one input value (p_0), but two (p_0, p_3). As p_3 is used as an input, the predicted pressure values at position p_3 are expected to correspond well with the measured pressures.

The origin of OSA syndrome is qualitatively explained by the negative pressure at the level of the constriction. As expected, an accurate quantitative model is obtained for the

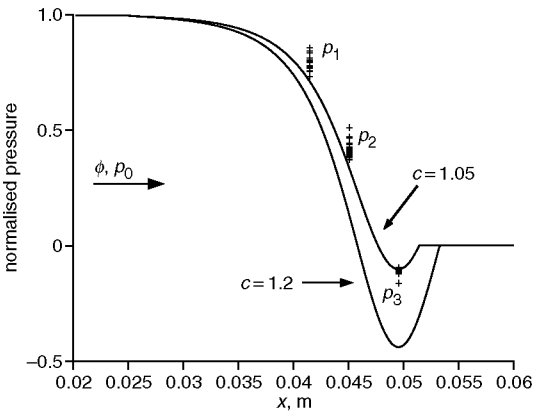

Fig. 7 *Pressure measurements along half cylinder at p_1, p_2 and p_3 (+) and Bernoulli simulations with $c = 1.05$ (solid line on top) and $c = 1.2$ (solid line below) normalised with upstream pressure p_0 for $h_{min} = 1.45$ mm and $\phi = 5$ l min^{-1} up to $\phi = 120$ l min^{-1}*

region of maximum pressure drop ($R^2 = 0.99$ at site p_3) from the 1D flow description. The impact of the *ad hoc* value c or the position of flow separation on the predicted pressure distribution is obvious. Consequently, the position of flow separation (or the value of the constant c) will largely affect the forces excerted by the flow on the surrounding tissues.

To evaluate further the retrieved constant $c = 1.05$, Fig. 9 shows the physical value of the constant c predicted using the Thwaites method and RNSP. It appears that the *ad hoc* value $c = 1.05$ greatly underestimates the position of flow separation x_S for all covered volume flow velocities. Therefore, although the *ad hoc* value $c = 1.05$ optimises the 1D modelling performance, it is an unphysical value resulting in a less accurate force distribution, as

$$F = W \int_{inlet}^{separation} p(x)\,dx \tag{10}$$

Therefore one-dimensional pressure prediction involving a fixed position of the flow separation point is not useful for application to OSA, where the force distribution is important, and will not be considered further. This finding is in agreement with PEDLEY and LUO (1998) and MATSUZAKI and FUNG (1976), who stress the importance of an accurate prediction of flow separation and the need to improve the one-dimensional model with more modern boundary layer methods.

Fig. 8 shows the measured and predicted longitudinal velocity profile along the x-axis using the Thwaites method and RNSP, outlined in Sections 2.2.2 and 2.2.3, for a steady flow of 40 l min^{-1} and with a minimum aperture $h_{min} = 3.00$ mm. Note the limited range of experimental data along the longitudinal dimension, i.e. the x-axis. This is owing to the physical dimensions of the hot film probe preventing further insertion inside the replica. The Thwaites method does not allow the computation of any predictions past the point of flow separation. Consequently, for large x values, only experimental datapoints and RNSP predictions can be seen. The same findings hold for all assessed minimum apertures and volume flow velocities.

The velocity values obtained with both the Thwaites method and RNSP are within 10% agreement with the measured velocity values, although the velocity distribution within the replica seems much more accurate with RNSP, as the trend in the measured data is captured.

5.2 *Pressure distribution*

The predictive value of the bidimensional flow predictions using the Thwaites method and RNSP is quantitatively explored. As the position of flow separation largly affects the force distribution, we reconsider the predicted values of the constant c for the different volume flow velocities depicted in Fig. 9. Altough very close, the constant predicted with Thwaites is systematically superior to the constant obtained from RNSP. Consequently, RNSP predicts flow separation to occur early compared with Thwaites, although, for all assessed minimum apertures, the difference in the predicted constant is small (<3%), except for small-volume flow velocities, where the difference increases up to $\pm 10\%$. To evaluate the prediction of the pressure distribution with Thwaites and RNSP, the pressures measured at positions p_1, p_2 and p_3 are compared with the computed pressures.

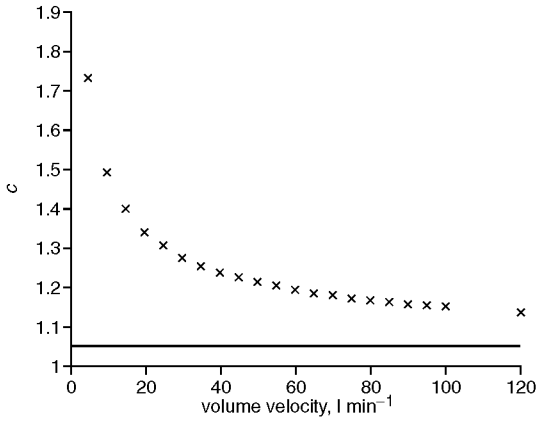

Fig. 9 *c as function of ϕ predicted from (▷) Thwaites, (×) RNSP and (—) ad hoc constant $c = 1.05$ for $h_{min} = 1.45$ mm*

Figs. 10–15 show the predicted and measured data normalised by the upstream pressure p_0 at positions p_1, p_2 and p_3 for, respectively, $h_{min} = 1.45$ mm and $h_{min} = 3.00$ mm, as a function of the upstream pressure p_0. In all Figures, the pressure drop predicted by RNSP is slightly superior to the pressure drop predicted by the Thwaites method. A larger pressure drop agrees with the slightly inferior value of the constant c mentioned earlier in the case of RNSP.

Figs. 12 and 15 illustrate that both Thwaites and RNSP pressure predictions at the minimum aperture p_3 yield well within the typically accepted error range of 25% on the measured pressure values (HOFMANS *et al.*, 2003). From the remaining Figures, it can be seen that this holds also for the pressure measured at positions p_1 and p_2. Note from Fig. 7 that using Bernoulli would give estimation errors far above the accepted error range of 25% if the position of flow separation was respected ($c = 1.2$).

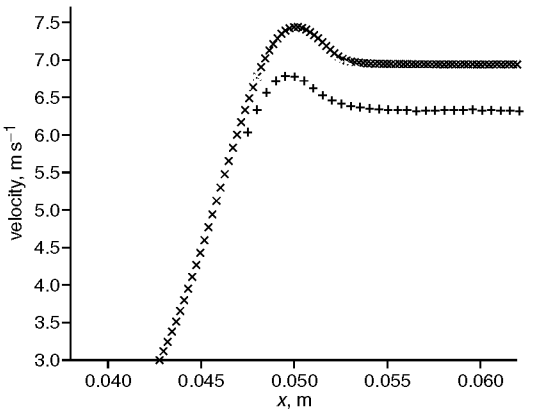

Fig. 8 *Longitudinal velocity profile with step of $\Delta x = 1.0$ mm for $h_{min} = 3.00$ mm and $\phi = 40$ l min^{-1}: (+) measured data, (▷) Thwaites and (×) RNSP*

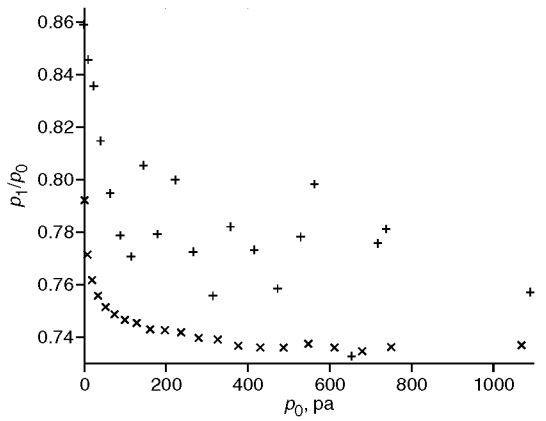

Fig. 10 *Normalised pressure at position p_1 for $h_{min} = 1.45$ mm: (+) measured data, (▷) Thwaites and (×) RNSP*

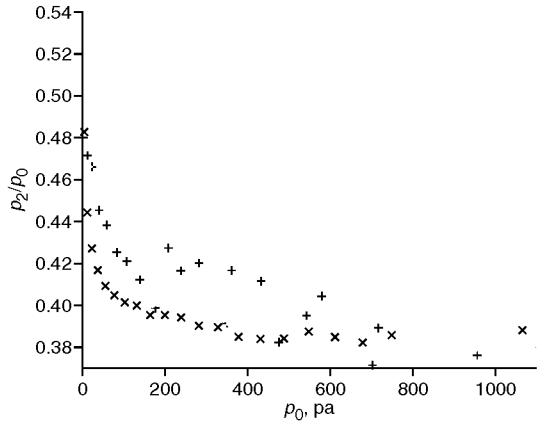

Fig. 11 *Normalised pressure at position p_2 for $h_{min} = 1.45$ mm: (+) measured data, (▷) Thwaites and (×) RNSP*

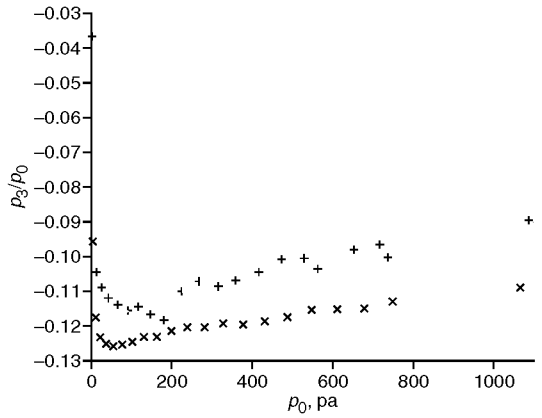

Fig. 12 *Normalised pressure position p_3 for $h_{min} = 1.45$ mm: (+) measured data, (▷) Thwaites and (×) RNSP*

The overall model performance for all assessed minimum apertures (1.45, 1.90, 2.30, 3.00 mm), at positions p_1, p_2 and p_3 for Thwaites and RNSP, is detailed in Table 2. The overall model accuracy is expressed by the mean coefficient of determination R^2 defined in (9), averaged for all minimum apertures and the indicated ranges of volume flow velocities extending from 5 l min^{-1} to, respectively, $\leqslant 30$, $\leqslant 60$, $\leqslant 80$, $\leqslant 100$ and $\leqslant 120$ l min^{-1}. The covered ranges allow us to evaluate the predictive value for distinct Reynolds numbers $Re = \phi/W\nu$, with ν being the kinematic viscosity coefficient and W and ϕ as defined previously. For all five cases, the

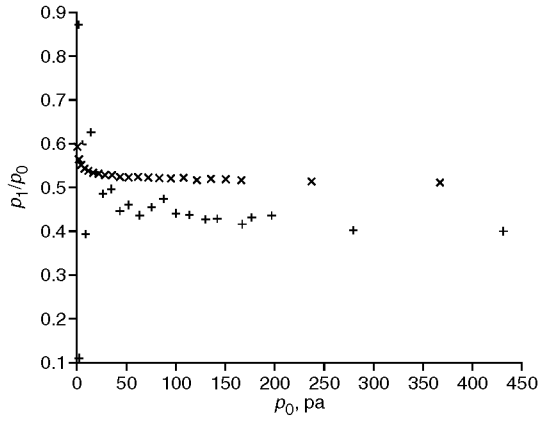

Fig. 13 *Normalised pressure at position p_1 for $h_{min} = 3.00$ mm: (+) measured data, (▷) Thwaites and (×) RNSP*

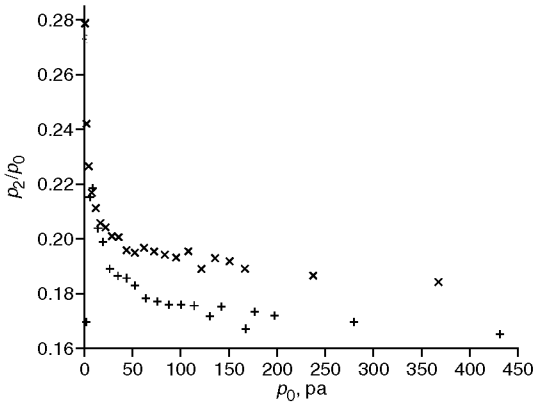

Fig. 14 *Normalised pressure at position p_2 for $h_{min} = 3.00$ mm: (+) measured data, (▷) Thwaites and (×) RNSP*

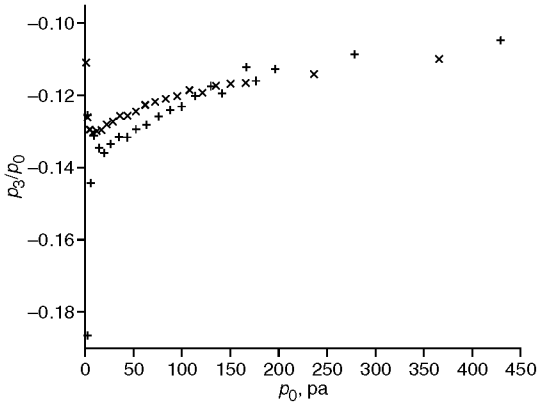

Fig. 15 *Normalised pressure at position p_3 for $h_{min} = 3.00$ mm: (+) measured data, (▷) Thwaites and (×) RNSP*

model performance of both Thwaites and RNSP at the position of minimum constriction $R^2_{p_3}$ is excellent ($R^2_{p_3} > 0.97$). Further, it can be seen that, in general, $R^2_{p_1} \leqslant R^2_{p_2} \leqslant R^2_{p_3}$. Thus R^2 and therefore the prediction performance increase approaching the position of minimum aperture. This finding stresses the importance of validating the pressure predictions at different sites along the replica to compare and evaluate flow predictions if the pressure distribution is of interest.

From Table 2, it follows that the model performance significantly increases for Reynolds numbers below ± 2500. Reynolds numbers below 2500 are characteristic of laminar flows. Higher values of the Reynolds number indicate the transition from laminar to turbulent flows. As the applied bidimensional flow predictions are laminar flow models, the flow behaviour was expected to be most accurately described within the laminar range, as is the case. Furthermore, the predictive value of RNSP slightly exceeds the Thwaites predictions for low-volume flow velocities in the laminar range. The volume flow velocities involved during OSA are below 30 l min^{-1} (FISHMAN *et al.*, 1986). Therefore, in the case of OSA, the predictive value of RNSP exceeds slightly the predictive value of the Thwaites method, and RNSP prediction is favoured to acquire the pressure distribution. This holds in particular for the position p_1, where the influence of the asymmetry is largest, although it can be seen that areas with the largest pressure drop will most contribute to the origin of OSA. Consequently, an accurate pressure prediction at the level of p_1 is least critical.

The present study experimentally confirms the numerical study reported in SHOME *et al.* (1998) for a rigid pharyngeal geometry and, in particular, the crucial effects of geometrical

Table 2 Overall Thwaites and RNSP prediction performance of steady pressure measurements at positions p_1, p_2 and p_3, averaged for all assessed minimum apertures, $h_{min} = 1.45$ mm, 1.90 mm, 2.30 mm and 3.00 mm, and indicated ranges of volume flow velocity

ϕ, l min^{-1}, Re, R^2	R^2 for p_1	R^2 for p_2	R^2 for p_3
$\phi \leqslant 120$ ($Re \leqslant 4719$)			
Thwaites	0.48	0.68	0.99
RNSP	0.50	0.71	0.97
$\phi \leqslant 100$ ($Re \leqslant 3140$)			
Thwaites	0.48	0.69	0.98
RNSP	0.52	0.71	0.97
$\phi \leqslant 80$ ($Re \leqslant 2510$)			
Thwaites	0.48	0.74	0.99
RNSP	0.57	0.77	0.97
$\phi \leqslant 60$ ($Re \leqslant 1888$)			
Thwaites	0.48	0.76	0.99
RNSP	0.61	0.82	0.98
$\phi \leqslant 30$ ($Re \leqslant 940$)			
Thwaites	0.53	0.80	0.99
RNSP	0.72	0.86	0.98

changes in the morphology. The minimum aperture or the degree of obstruction on the pressure drop is systematically varied to explore the influence of small geometrical changes, as, for example, caused by surgery. In addition, the applied *in vitro* methodology allows validation of major theoretical hypotheses and quantification of the flow model performance. As measuring flow characteristics and, hence, theoretical model validation inside an oscillating elastic tube are a difficult tasks, the presented study is a necessary step towards flow modelling in the case of a non-rigid collapsible replica. Experimental validation under controlled and measurable experimental conditions on a non-rigid elastic replica is the next crucial step before extending the findings to a real human pharynx and prediction of surgical interventions.

6 Conclusions

As a first step towards the physical modelling of obstructive sleep apnoea, some flow assumptions and resulting flow predictions have been experimentally and quantitatively assessed. A rigid *in vitro* pharyngeal tongue replica was developed so that we could study the flow through a characteristic asymmetrical constriction.

It is shown from a dimensionless analysis that, in the first approximation, the fluid flow through the *in vitro* replica can be described as steady and incompressible. Measured velocity profiles and measured pressures at different places along the converging part of the constriction confirmed the relevance of a bidimensional flow description, whereas the viscous pressure losses can be neglected outside the boundary layer. Furthermore the velocity profiles revealed an asymmetry of the flow downstream from the constriction, owing to the geometrical asymmetry. However, transverse pressure measurements on both sides of the constriction showed that the influence of the asymmetry on the measured pressure within the constriction was negligible. This point was further confirmed by considering the predictions obtained by a two-dimensional flow description from the boundary layer solution and reduced Navier Stokes simulations. The use of these two-dimensional flow descriptions resulted in a physical prediction of the position of flow separation.

It was found that the general behaviour of the *in vitro* model was different from that of the classical Starling resistor (LAMBERT and WILSON, 1972). As a matter of fact, the outcome of a classical one-dimensional flow description is sufficient in applications where only prediction of the volume flow is sought, but it fails to predict the pressure distribution. Therefore the one-dimensional flow description is not suitable to describe the forces acted on surrounding structures by the flow, which is needed when obstructive sleep apnoea is considered. Quantitative experimental validation shows that, both for the bulk velocity and for the pressure distribution, two-dimensional flow descriptions yield pressure predictions with an accuracy of 15%. Application of the reduced Navier Stokes equations is slightly favoured, as they allow us to account for the asymmetry in the geometry.

Further work is needed to evaluate, theoretically and experimentally, unsteady effects owing to flow fluctuation or wall deformation.

Acknowledgment—The authors would like to thank Pierre Chardon, Franz Chouly, Yohan Payan and the two anonymous reviewers for their valuable contributions and comments.

The work is part of an Emergence project granted by the CNRS federations ELESA/IMAG and the Rhône-Alpes region, France.

References

AYAPPA, I., and RAPOPORT, D. (2003): 'The upper airway in sleep: physiology of the pharynx', *Sleep Med. Rev.*, **7**, pp. 9–33

BLEVINS, R. (1992): 'Applied fluid dynamics handbook' (Krieger Publishing Company, Malabar, 1992)

BRIDGMAN, S., and DUNN, K. (2002): 'Surgery for obstructive sleep apnoea', *Cochrane Database Syst. Rev.*, **2**, CD001004

DEVERGE, M., PELORSON, X., VILAIN, C., LAGREE, P., CHENTOUF, F., WILLEMS, J., and HIRSCHBERG, A. (2003): 'Influence of collision on the flow through in-vitro rigid models of the vocal folds', *J. Acoust. Soc. Am.*, **114**, pp. 1–9

FISHMAN, A., MACKLEM, P., MEAD, J., and GEIGER, S. (1986): 'The respiratory system', in 'Handbook of physiology' (Am. Phys. Soc., Maryland, 1986)

FLEMONS, W. (2002): 'Obstructive sleep apnea', *New Engl. J. Med.*, **347**, pp. 498–504

FLEMONS, W., and REIMER, M. (2002): 'Measurement properties of the calgary sleep apnea quality of life index', *Am. J. Respir. Crit. Care Med.*, **165**, pp. 159–164

GROTBERG, J., and JENSEN, O. (2004): 'Biofluid mechanics in flexible tubes', *Ann. Rev. Fluid Mech.*, **36**, pp. 121–147

HENKE, K. (1998): 'Upper airway muscle activity and upper airway resistance in young adults during sleep', *J. Appl. Physiol.*, **84**, pp. 486–491

HOFMANS, G., GROOT, G., RANUCCI, M., and GRAZIANI, G. (2003): 'Unsteady flow through *in-vitro* models of the glottis', *J. Acoust. Soc. Am.*, **113**, pp. 1658–1675

HUI, D., CHOY, D., KO, F., LI, T., and LAI, C. (2000): 'Obstructive sleep apnoea syndrome: treatment update', *Med. Pract.*, **6**, pp. 209–217

LAMBERT, K., and WILSON, T. (1972): 'Flow limitation in a collapsible tube', *J. Appl. Physiol.*, **33**, pp. 150–153

LEITH, D. (1995): 'Cough', *Eur. Respir. J.*, **8**, pp. 1993–1202

LIPTON, A., and GOZAL, D. (2003): 'Treatment of obstructive sleep apnea in children: do we really know how?', *Sleep Med. Rev.*, **7**, pp. 61–80

MANSOUR, K., ROWLEY, J., MESHENISH, A., SHKOUKANI, M., and BADR, M. (2002): 'A mathematical model to detect inspiratory flow limitation during sleep', *J. Appl. Physiol.*, **93**, pp. 1084–1092

MATSUZAKI, Y., and FUNG, Y. (1976): 'On separation of a divergent flow at moderate Reynolds numbers', *ASME J. Appl. Mech.*, **43**, pp. 227–231

MAYER, P., PEPIN, J., BETTEGA, G., VEALE, D., FERRETI, G., DESCHAUX, C., and LEVY, P. (1996): 'Relationship between body mass index, age and upper airway measurements in snorers and sleep apnea patients', *Eur. Respir. J.*, **9**, pp. 1801–1809

MCNICHOLAS, W. (2003): 'Sleep apnoea syndrome today: much done, more to do', *Sleep Med. Rev.*, **7**, pp. 1087–1093

PAYAN, Y., CHABANAS, M., PELORSON, X., VILAIN, C., LEVY, P., LUBOZ, V., and PERRIER, P. (2002): 'Biomechanical models to stimulate consequences of maxillofacial surgery', *C. R. Biol.*, **325**, pp. 407–417.

PEDLEY, T., and LUO, X. (1998): 'Modelling flow and oscillations in collapsible tubes', *J. Theor. Comp. Fluid Dyn.*, **10**, pp. 277–294

PELORSON, X., HIRSCHBERG, A., HASSELT, R. V., WIJNANDS, A., and AUREGAN, Y. (1994): 'Theoretical and experimental study of quasi steady-flow separation within the glottis during phonation. Application to a modified two-mass model', *J. Acoust. Soc. Am.*, **96**, pp. 3416–3431

PENZEL, T., MCNAMES, J., DE CHAZAL, P., RAYMOND, B., MURRAY, A., and MOODY, G. (2002): 'Systematic comparison of different algorithms for apnoea detection based on electrocardiogram recordings', *Med. Biol. Eng. Comput.*, **40**, pp. 402–407

PEPPARD, P., YOUNG, T., PALTA, M., and SKATRUD, J. (2000): 'Prospective study of the association between sleep-disordered breathing and hypertension', *New Engl. J. Med.*, **342**, pp. 1378–1374

RAMA, A., TEKWANT, S., and KUSHIDA, C. (2002): 'Sites of obstruction in obstructive sleep apnea', *Chest*, **122**, pp. 1139–1147

SCHLICHTING, H., and GERSTEN, K. (2000): 'Boundary layer theory' (Springer Verlag, Berlin, 2000)

SCHWAB, R., GEFTER, W., HOFFMAN, E., GUPTA, K., and PACK, A. (1990): 'Dynamic upper airway imaging during awake respiration in normal subjects and patients with sleep disordered breathing', *Am. J. Respir. Crit. Care Med.*, **148**, pp. 1385–1400

SHER, A., SCHECHTMAN, K., and PICCIRILLO, J. (1996): 'The efficacy of surgical modifications of the upper airway in adults with obstructive sleep apnea syndrome', *Sleep*, **19**, pp. 156–177

SHOME, B., WANG, L., SANTARE, M., PRASAD, A., SZERI, A., and ROBERTS, D. (1998): 'Modeling of airflow in the pharynx with application to sleep apnea', *J. Biomech. Eng.*, **120**, pp. 416–422

TERAN-SANTOS, J., JIMINEZ-GOMEZ, A., CORDERO-GUEVARA, J. (1999): 'The association between sleep apnea and the risk of traffic accidents', *New Engl. J. Med.*, **340**, pp. 847–851

YOUNG, T., PALTA, M., DEMPSEY, J., SKATRUD, J., WEBER, S., and BADR, S. (1993): 'The occurrence of sleep-disordered breathing among middle-aged adults', *New Eng. J. Med.*, **17**, pp. 1230–1235

Authors' biographies

ANNEMIE VAN HIRTUM received the PhD degree in Physics at the Katholieke Universiteit Leuven, Belgium in 2002. After being a post-doctoral fellow at the Institut de la Communication Parlée, France she became a CNRS researcher in 2004. Her research interest is focused on the physical understanding of flow related phenomena in the respiratory system.

XAVIER PELORSON received a PhD in physical acoustics from the University of Maine, France in 1991. After a two years post-doc at the laboratory for fluid mechanics of the Technical University of Eindhoven, he became a fellow researcher at the CNRS. His main research interests concern the physical modelling of the human voice and of the upper airways.

PIERRE-YVES LAGRÉE, studied at the Ecole Normale Supérieure de Saint Cloud between 1985 and 1989, received the Agrégation of Physics in 1988 and his PhD in 1992. Since 1992, he has been a CNRS Researcher in Fluid Mechanics at University Paris VI, and teaches thermal flows at ENSTA (Engineering School, Paris). His research interests include all boundary layer flows with applications in biomechanics.